Spectral mixture analysis of EELS spectrum-images.

Nicolas Dobigeon, Nathalie Brun

Spectral mixture analysis of EELS spectrum-images

Nicolas Dobigeon [a], Nathalie Brun [b,*]

[a] University of Toulouse, IRIT/INP-ENSEEIHT, 2 rue Camichel, 31071 Toulouse Cedex 7, France
[b] University of Paris Sud, Laboratoire de Physique des Solides, CNRS, UMR 8502, 91405 Orsay Cedex, France

Keywords:
Electron energy-loss spectroscopy (EELS)
Spectrum imaging
Multivariate statistical analysis
Spectral mixture analysis

A B S T R A C T

Recent advances in detectors and computer science have enabled the acquisition and the processing of multidimensional datasets, in particular in the field of spectral imaging. Benefiting from these new developments, Earth scientists try to recover the reflectance spectra of macroscopic materials (e.g., water, grass, mineral types…) present in an observed scene and to estimate their respective proportions in each mixed pixel of the acquired image. This task is usually referred to as *spectral mixture analysis* or *spectral unmixing* (SU). SU aims at decomposing the measured pixel spectrum into a collection of constituent spectra, called *endmembers*, and a set of corresponding fractions (*abundances*) that indicate the proportion of each endmember present in the pixel. Similarly, when processing spectrum-images, microscopists usually try to map elemental, physical and chemical state information of a given material. This paper reports how a SU algorithm dedicated to remote sensing hyperspectral images can be successfully applied to analyze spectrum-image resulting from electron energy-loss spectroscopy (EELS). SU generally overcomes standard limitations inherent to other multivariate statistical analysis methods, such as *principal component analysis* (PCA) or *independent component analysis* (ICA), that have been previously used to analyze EELS maps. Indeed, ICA and PCA may perform poorly for linear spectral mixture analysis due to the strong dependence between the abundances of the different materials. One example is presented here to demonstrate the potential of this technique for EELS analysis.

1. Introduction

Over the two last decades, scanning transmission electron microscopy (STEM) has benefit from important advances in electron-based instrumentation and technology. These recent advances have enabled the development of electron energy-loss spectroscopy (EELS). EELS provide spectrum-images, that have been widely used in various applications, including material science and chemical analysis [1,2]. The multidimensional data coming from EELS analysis exploit inherent spatial information to build elemental maps. An elemental map is useful per se, however it does not exploit additional crucial information present in the acquired spectrum image. As EELS signal is sensitive to chemical changes and atom environment, building a map of the different materials would be more much more relevant. Therefore, there is a real need for efficient techniques to process EELS spectrum-images, able to identify and quantify the spectral components that represent the different compounds present in the imaged sample.

Attempts to extract information from EELS spectra were conducted in 1999 mainly based on multivariate data analysis techniques, specifically principal component analysis (PCA) [3]. A PCA-based method was written for DigitalMicrograph and commercialized by Ishizuka in 2001 [4] and is now rather widely used for data filtering and dimensional reduction [5]. However, such analysis faces the difficulty of extracting physically meaningful spectra from the computed eigenvalues.

Conversely, independent component analysis (ICA) aims at identifying statistically independent components from multivariate data. In 2005, Bonnet and Nuzillard [6] applied the ICA-based SOBI algorithm to process spectrum image data set. The authors noticed that, since EELS spectra are not composed of separated peaks, the independence hypothesis is not fulfilled. To overcome this issue, successive derivatives of EELS-spectra are analyzed. From this analysis, it seems that first derivatives produce more interpretable results than second derivatives. Unfortunately, this finding was empirical and no theoretical argument was found to justify this point. De La Peña proposed in [7] to use a kernelized version of ICA. This approach allows C, SnO_2 and TiO_2 signals to be successfully separated while analyzing a spinodally decomposed solid solution. Satisfactory quantitative analysis was obtained but no fine structure analysis was performed. The authors noticed that difficulties could be encountered because of multiple scattering and energy instabilities introducing non linearity.

Recently a matrix factorization technique has been proposed to map plasmon modes on silver nanorods [8]. The analysis, relying on the software AXSIA developed by Keenan [9] consists in looking for a rotation matrix to be applied on orthogonal factors to maximize the intrinsic "simplicity" of the decomposition.

* Corresponding author. Tel.: +33 1 69 15 53 80.
E-mail address: nathalie.brun@u-psud.fr (N. Brun).

Specifically, the optimal solution is defined by the sparsity of the spatial distribution of each individual material.

In a significantly different area – namely remote sensing and geoscience – reflectance spectroscopy is widely used to characterize and discriminate materials on the Earth surface for various applications [10]. Usually mounted on aircrafts, balloons or satellites, spectral sensors collect electromagnetic radiations from the Earth surface. Most of the recorded signals are reflectance spectroscopic signals measured in the infra-red/visible range. The collection of these signals over an observed scene provides a multi-band image formed as a 3-dimensional data cube. Each pixel of the atmospheric-corrected image is characterized by a vector of reflectance measurements. Specifically, *hyperspectral* images are composed of pixels with several hundreds of narrow and contiguous spectral bands.

Faced with this amount of data, the geophysicist community has developed analysis methods to extract physical information from these images. One of the main objectives of these methods is to identify spectral properties corresponding to distinct materials in a given scene and thus to get classification maps of the image pixels. However, because of the intrinsically limited spatial resolution of the hyperspectral sensors, several materials (e.g., water, grass, mineral types…) usually contribute to the spectrum measured at a given single pixel. The resulting spectral measurement is a combination of the individual spectra that are characteristic of the macroscopic materials. Consequently, techniques to estimate the constituent substance spectra and their respective proportions from mixed pixels are needed. *Spectral unmixing* is the procedure that aims at (i) decomposing the measured pixel spectrum into a collection of constituent spectra, or *endmembers*, and (ii) estimating the corresponding fractions, or *abundances*, that indicate the proportion of each endmember present in the pixel [11].

What is usually known as «spectrum image» in the microscopist community corresponds very precisely to a «hyperspectral image» for the geoscience-related applications. The analogy between these two fields of research is undeniable. However, at the present time microscopists are less advanced in their ability of conducting efficient multivariate analysis of their data. In this work we describe how a recent spectral unmixing algorithm developed by Dobigeon et al. [12] for analyzing hyperspectral images can be successfully applied to spectrum images resulting from EELS maps.

2. Methods and experimental setup

2.1. Spectral mixture analysis

This paragraph formulates the so-called spectral unmixing or spectral mixture analysis. Let **Y** denote the L by N observed data matrix that gathers the whole set of N measured pixel spectra. Each column of the **Y** is a vector of size L which corresponds to the reflectances measured in the L spectral bands. The spectral mixture analysis (SMA) conducted on the spectrum image consists of decomposing this matrix **Y** into a product matrix **SA**. In this decomposition scheme, each column of the L by R matrix **S** is the spectral signature of a constituent (endmember). Conversely, each column of **A** is a set of R coefficients corresponding to the relative proportions of the signatures in the pixels. Thus, like any factorization matrix method, SMA estimates the two latent variables **S** and **A** leading to the product **SA** that best approximates the observed matrix **Y**. Since this decomposition is non-unique, the problem of estimating **S** and **A** from **Y** is ill-conditioned. To reduce the set of admissible solutions, additional constraints on **S** and **A** are considered. First, as any non-negative matrix factorization (NMF) approach, the elements of **S** and **A** are assumed to be positive. Moreover, since the coefficients in each column of **A** represent proportions, it is natural to consider an additional sum-to-one constraint on these columns. This constrained

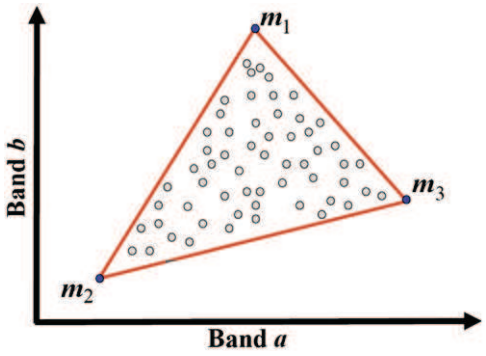

Fig. 1. Geometrical formulation of spectral mixture analysis (SMA). The scatterplot represents the data observed in a 2-D space. The mixed pixels (gray circles) belong to the simplex (simplest geometric figure that is not degenerate in n-dimensions), whose vertices are the 3 endmembers. SMA algorithms exploit different properties of the simplex.

matrix factorization problem has been widely addressed in the geoscience and remote sensing literature since SMA is a crucial step in analyzing multi-band images, e.g., hyperspectral data. Note that, from a geometrical point of view, SMA consists of identifying the vertices of a lower dimensional simplex formed by the observed data (Fig. 1). Indeed, under the positivity and additivity constraints introduced previously, the observed spectral vectors form a simplex whose vertices correspond to the endmembers to be identified. $R+1$ pure endmembers spectra form the vertices of an R-simplex. Thus, as examples, a 2-simplex is a triangle (Fig. 1), a 3-simplex a tetrahedron… Several algorithms of the geoscience and remote sensing literature have proposed to exploit this geometrical formulation to solve the spectral unmixing problem. Vertex Component Analysis (VCA) is one of the most popular geometric algorithm [13]. It consists of iteratively (i) projecting the data onto the direction orthogonal to the subspace spanned by the endmembers previously identified (ii) assigning the extreme projection as a new endmember.

Geometrical algorithms have the great advantage of being computationally efficient. However, most of them, such as VCA, rely on the hard hypothesis of "pure pixels", i.e., they assume that the endmembers are present among the observed pixels. Unfortunately, this assumption can be rarely ensured and alternative strategies must be considered.

In this work, SMA is conducted with the Bayesian Linear Unmixing (BLU) method proposed by Dobigeon et al. [12]. Originally developed to address the hyperspectral unmixing of remote sensing images, BLU relies on a Bayesian formulation of the estimation problem. This Bayesian framework allows the positivity and sum-to-one constraints introduced above to be conveniently included into the observation model.

The proposed BLU method has the great advantage of recovering the endmember signatures **S** and their respective proportions **A** jointly in a single step. Naturally, this strategy casts SMA as a standard blind source separation (BSS) problem. Moreover, contrary to geometrical based algorithm like VCA, it does not require the assumption of having pure pixels among the data. Moreover, note that BLU solves the endmember estimation problem directly on a lower dimensional space, exploiting the intrinsic geometrical interpretation of SMA noticed above. By conducting SMA in the subspace spanned by the identified simplex, the number of freedom associated with the parameters to be estimated is significantly reduced when compared to other algorithms dedicated to SMA.

The methodology of BLU can be summarized as follows. First, appropriate prior distributions $p(\mathbf{S})$ and $p(\mathbf{A})$ are assigned to the unknown parameters **S** and **A**, respectively. These distributions are chosen to ensure the positivity and sum-to-one constraints imposed on the unknown matrices **S** and **A**. Then, based on this prior modeling

and the well-admitted assumption of a Gaussian likelihood $p(\mathbf{Y}|\mathbf{S},\mathbf{A})$, the joint posterior distribution $p(\mathbf{S},\mathbf{A}|\mathbf{Y})$ is computed using the Bayes paradigm. Unfortunately, this posterior is too complex to easily derive the closed-form expressions of the standard Bayesian estimators, such as the maximum a posteriori or posterior mean. Consequently, a Markov chain Monte Carlo (MCMC) algorithm is designed to generate samples $\mathbf{S}^{(t)}$ and $\mathbf{A}^{(t)}$ ($t=1,\ldots$NMC) asymptotically distributed according to the posterior of interest. Finally, the Bayesian estimators of the endmember matrix $\mathbf{S}$ and the proportion matrix $\mathbf{A}$ are then approximated using these NMC generated samples. Note that a Matlab© code of the BLU algorithm is freely available online [12].

2.2. Experimental data

In the following sections, SMA of a spectrum-image of nanoparticles is conducted. More precisely, the ability of BLU to provide interpretable spectral signatures is demonstrated, thus overcoming the standard limitations inherent to other multivariate analysis techniques, such as PCA and ICA.

The analyzed dataset consists of a 64×64 pixel spectrum-image acquired in 1340 energy channels over a region composed of several nanocages in a boron-nitride nanotubes (BNNT) sample. Note that nanocages are supported by a holey carbon film for TEM analysis. These data have been extensively described and analyzed in [14] and a high angle dark field image of the region of interest is depicted in Fig. 2. In this study, ELNES «fingerprints» for different bonding configurations of boron (B–B, B–O, B–$N^{\pi*}$, B–$N^{\sigma*}$) have been extracted from selected area of the sample. Then reconstructed spectra are computed according to a linear combination of a power law and four fingerprints thanks to a multiple least squares fitting procedure. Fig. 3 displays characteristic spectra with the involved edges (B–K, C–K, N–K and O–K).

3. Results

3.1. Principal component analysis

PCA has demonstrated its ability to extract relevant information from multidimensional data. For instance, this method and its application to EELS data have been described in [3]. Moreover, this powerful multivariate analysis technique is also able to provide a minimal representation of the signal of interest, performing an explicit dimensionality reduction. In particular, in the specific context of SMA and according to the geometrical interpretation of spectral unmixing given in the previous section,

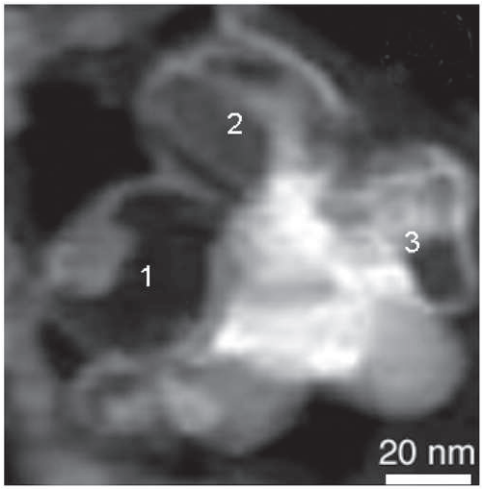

Fig. 2. HADF image corresponding to a 64×64 spectrum-image recorded in an area rich in nanoparticles containing boron (pure boron, boron oxide or h-BN).

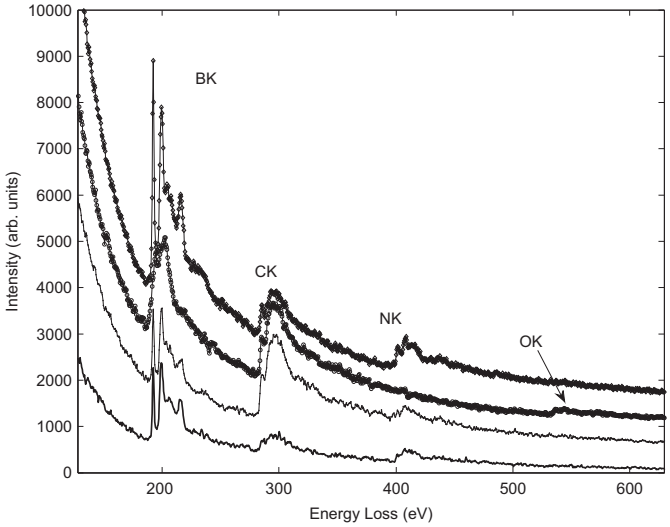

Fig. 3. Typical EELS spectra extracted from the 64×64 spectrum image in Fig. 2. Boron, carbon, nitrogen and oxygen K edges are represented.

the intrinsic dimension of the data is straight related with the number of endmembers to be recovered. When the mixed pixels are assumed to be obtained from the constrained linear combination of R spectral components, only R-1 dimensions are required to represent the data without loss of any information.

The method commonly advocated to determine the intrinsic dimensional of the data is to monitor the eigenvalues obtained by PCA. Only eigenvectors associated with eigenvalues of highest magnitudes are retained as significant contributions. Several criteria have been proposed to decide on the number of relevant eigenvalues. One solution consists in plotting the logarithm of these eigenvalues previously arranged in decreasing order. Ideally, smallest values related to noise correspond to the final linear part of the plot. However, the actual dimensionality of the data is generally difficult to assessed in practice, since changes between two adjacent eigenvalues may not be significant. This is typically the case for real data encountered in hyperspectral imagery, such as the HYDICE image scene. In [15], the authors conclude that only a crude estimate of the number of signal sources can be provided. Indeed the signature of an unique target may vary significantly from one area to another. Moreover, signal of weak amplitude might be difficult to separate from noise.

The eigenvalues for the analyzed spectrum-image are plotted in Fig. 4. As expected, the threshold cannot be clearly defined since there is no drastic drop in the eigenvalues distribution. The main objective of the study is to separate B–$N^{\pi*}$ from B–$N^{\sigma*}$ while keeping a minimum number of components for the other signatures. In practice, the analysis of the considered EELS dataset has been conducted with a number of spectral signatures R ranging from 6 to 8 for each evaluated analysis method (PCA, ICA and SMA).

PCA has been performed with $R=8$ using the open source Hyperspy toolbox [7], with a weighted version of PCA. The first eight spectra corresponding to PCA eigenvectors of highest relevance are displayed in Fig. 5. It clearly appears that these components do not correspond to any meaningful physical spectra. Consequently, they do not allow any interpretation, quantification or comparison with reference spectra. This can be explained by the fact that PCA searches for orthogonal components, which is not a realistic assumption for EELS application.

3.2. Independent component analysis

Whereas PCA searches for orthogonal components, ICA aims at identifying statistically independent components. Different

measures of independence have been exploited in the literature, corresponding to different algorithms. In this work ICA has been performed using the open source Hyperspy toolbox [7], choosing the CubICA algorithm. In contrast to other ICA methods, CubICA can be used without any parameter adjustments. It is thus easy to use and has been already applied for EELS spectrum-imaging data analysis. After visual expertise of the results obtained for $R=6$, $R=7$ and $R=8$ components, we considered that $R=7$ provides the most physically interpretable results. The identified components and their respective abundance maps are depicted in Figs. 6 and 7, respectively. The component IC5 is clearly identified as amorphous carbon and the map corresponds to the carbon supporting film. The 3 components IC1, IC4 and IC7 are associated with pure Boron and the corresponding abundance maps match those obtained in [14] for this specific compound. The separation of the signature into 3 different components may be explained by thickness effects. By analyzing the abundance map associated with IC2, this component can be identified as B–N$^{\pi*}$, but its features are significantly different from those of the reference spectrum in [14] and do not correspond to any proper EELS edge. Similarly IC3 should correspond to B_2O_3. However, whereas O–K edge appears properly, no real physical edge for the B–K is obtained. Finally, unfortunately, component IC6 does not correspond to physically acceptable spectra and its abundance map is not interpretable. As a consequence, we have to conclude that ICA has failed to completely unmix the signal sources. In particular, we do not obtain the signature for B–N$^{\pi*}$, B–N$^{\sigma*}$. This limitation of ICA has already been noticed in [16]. Note that considering other numbers of components does not significantly improve the results.

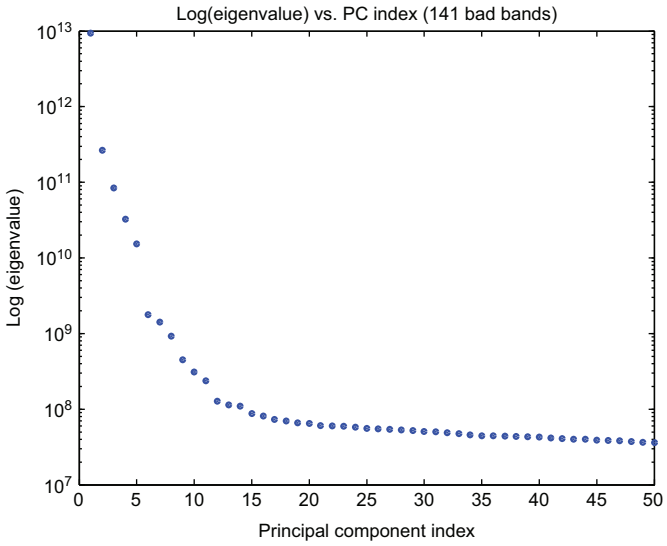

Fig. 4. Principal component eigenvalues for the analyzed spectrum-image arranged in a decreasing order (depicted in logarithmic scale). The threshold between eigenvalues associated signal and those associated with noise is not easy to determine. Indeed, there is no drastic drop in the eigenvalue distribution. In this work, the intrinsic dimensionality of the data is estimated around 7.

We also tried to perform the analysis by restricting the energy range to a window corresponding to B–K edge, i.e., 188–206 eV, following the strategy in [14]. However, once again, ICA fails to unmix properly the components. By choosing the energy range 330–610 eV, which only corresponds to Ca, N and O, satisfying unmixing results can be obtained with 4 components: background, BN, B_2O_3 and pure boron (Figs. 8 and 9). In this case, the differences between the two orientations of h-BN are too small to be detected on the N–K edge, providing only one component for h-BN. Consequently, it seems that ICA performs better with high energy ranges, as it was the case in [7] with a 430–800 eV energy window. According to [7],

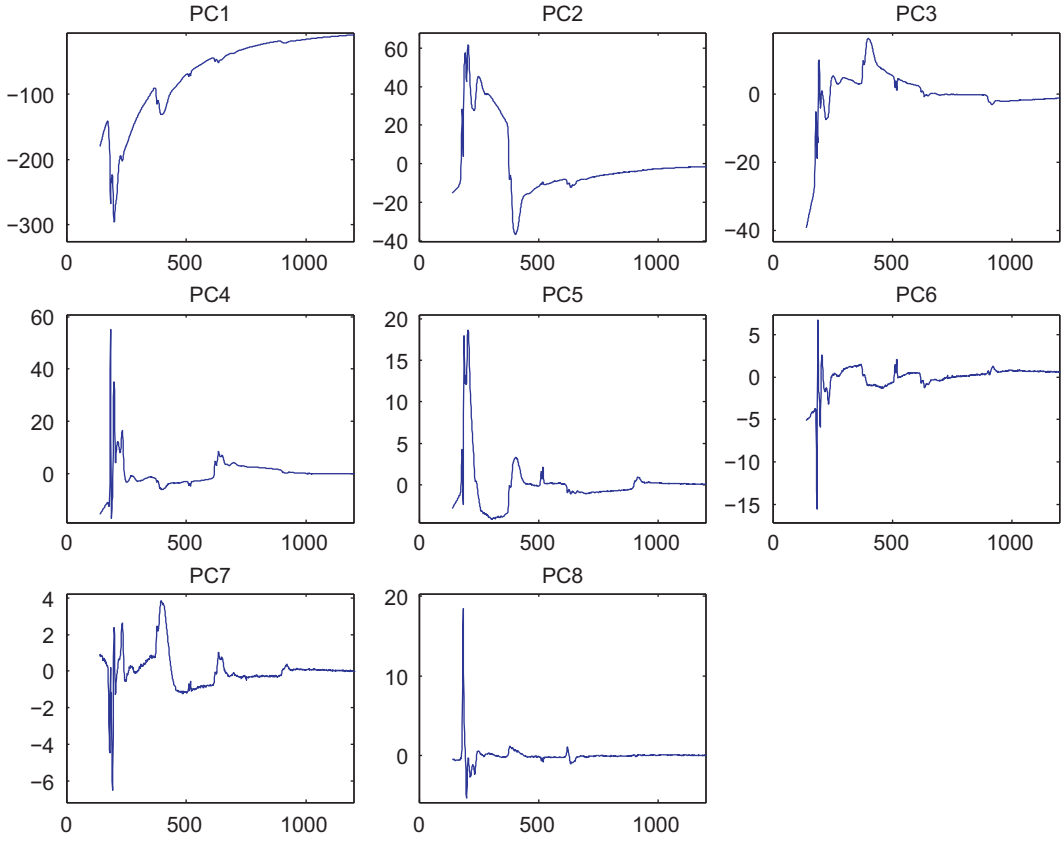

Fig. 5. First 8 most relevant components determined by PCA. These components are orthogonal and thus do not correspond to any "physically" significant spectral signature.

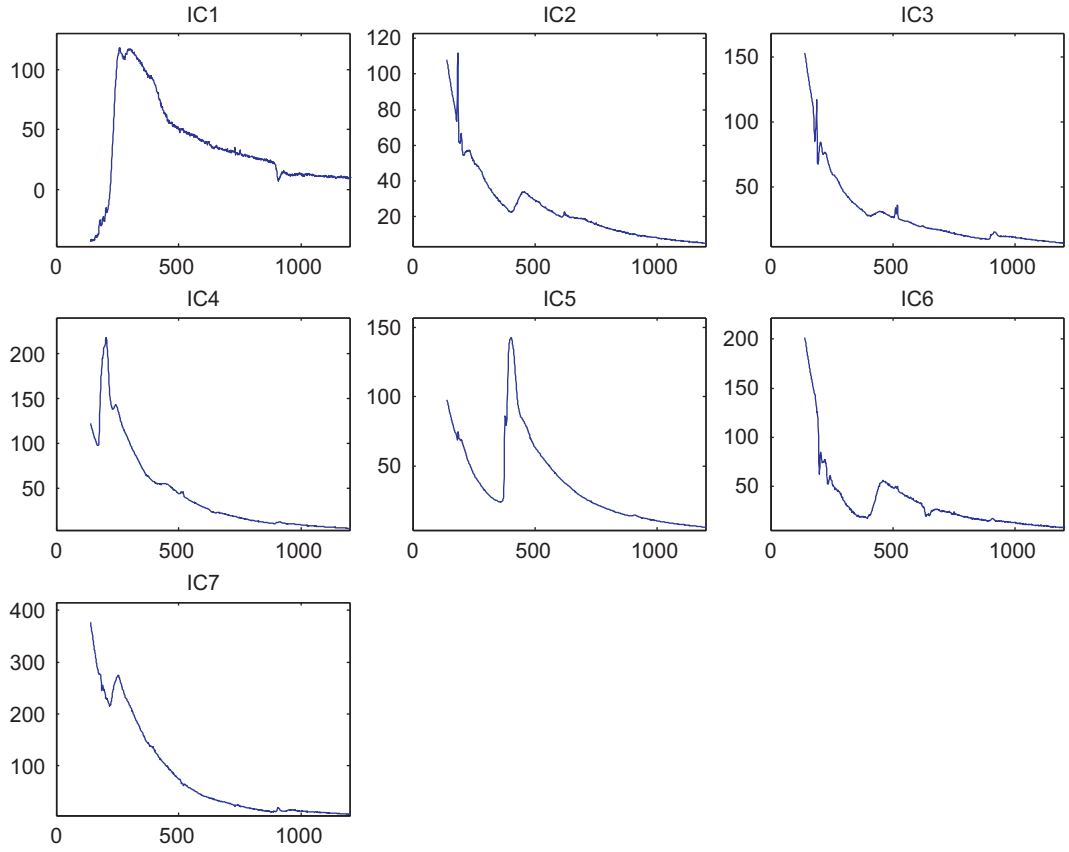

Fig. 6. Spectral components extracted by CubICA. Some components are completely different from the reference spectra and have no physical meaning. The corresponding maps are depicted in Fig. 7.

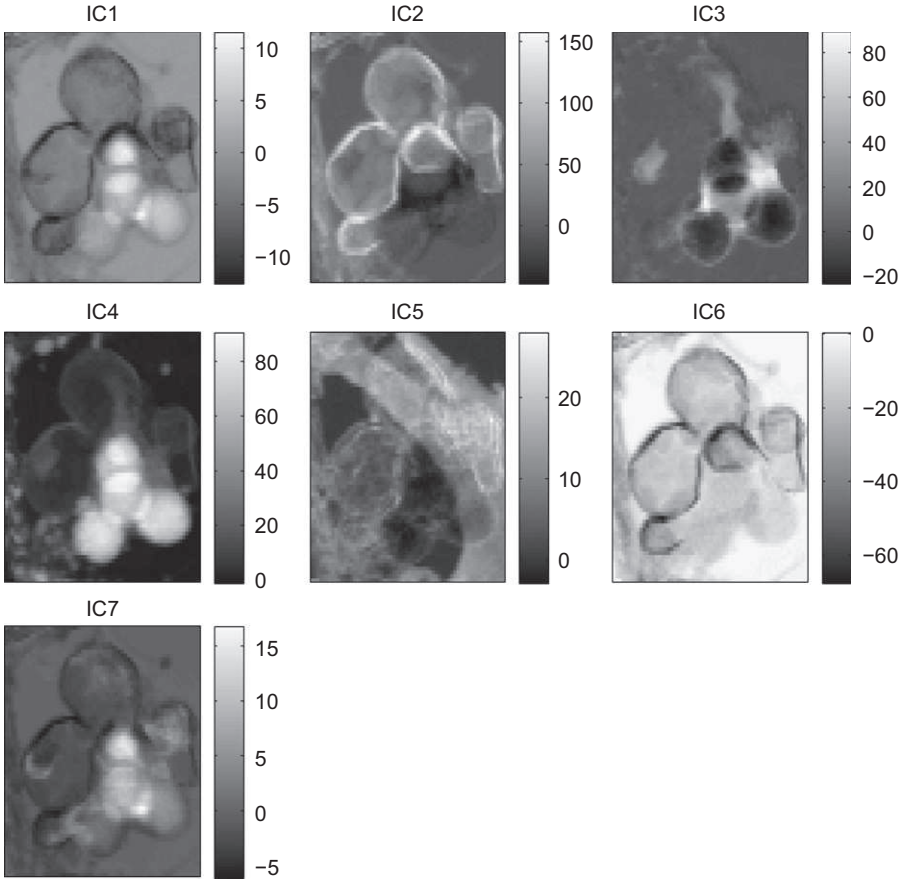

Fig. 7. Maps of the spectral components extracted by CubICA (the spectral signatures are depicted in Fig. 6).

this could be explained by non-linear effects caused by multiple scattering and by the variance of the C–K edge which is of the same order of magnitude as the other signals. In the analyzed example, since B–K is the edge of interest, the energy levels that contain this non-linearity cannot be removed from the analysis without losing crucial and discriminative information initially contained in the data.

3.3. Spectral mixture analysis with VCA and BLU

SMA of the EELS spectrum-imaging data is conducted by using the BLU algorithm presented in paragraph 2.1. We found that $R=8$ give the most satisfying results. The BLU algorithm has been initialized with endmembers provided by the VCA algorithm introduced in Section 2.1. Unmixing results provided by VCA are also reported to be compared with endmembers identified by BLU. VCA and BLU calculations were performed in the Matlab® (Release 2010b) environment.

Results obtained with VCA are presented in Figs. 10 and 11. It clearly appears that (i) all spectra correspond to realistic EELS spectra with characteristic edges on a decreasing background, and (ii) the related maps correctly separate different areas on the sample, which was not the case for maps obtained with ICA. The comparison of maps and endmembers with results obtained in [14] allows some target signature to be easily identified:

- According to the C map of [14], component VCA1 corresponds to the C supporting film.
- VCA2 and VCA6 both correspond to pure B in [14]. This is similar to the case of AVIRIS hyperspectral data where the «playa» signature is separated into two distinct regions [15]. It is likely that the splitting of the pure-B component does not correspond to 2 physically distinct signals.
- VCA3 is related to holes in the sample, thus there is no characteristic signal. This component is nevertheless necessary to account for the absence of signal in these pixels.
- VCA4 corresponds to B–N$^{\sigma*}$ but the map is slightly different from the one obtained in [14].
- VCA5 can be associated with B_2O_3 since fine structure in the corresponding abundance map the presence of O are in good agreement with results obtained in [14] for boron oxide.
- Component VCA7 corresponds to B–N$^{\pi*}$, with a observable N–K edge.

The endmember spectra estimated by the proposed BLU algorithm are depicted in Fig. 12 and the abundance maps in Fig. 13. For some components, results are quite similar to those obtained with VCA.

- VCA7 and BLU7 correspond to B–N$^{\pi*}$ with an identifiable N–K edge.
- VCA4 and BLU4 correspond to B–N$^{\sigma*}$.
- VCA1 and BLU1 correspond to the C supporting film.
- Pure B is separated into two components, BLU2 and BLU6 (VCA2 and VCA6, respectively).

However some endmembers unmixed by BLU are significantly different.

- Whereas B–O signature was divided into 2 distinct components with VCA (VCA5 and VCA8), BLU is able to identify only one spectral signature with a strong O signal (BLU5).
- Vacuum signal is classified into 2 components (BLU3 and BLU8).

This later feature is quite difficult to be interpreted. When applied with only 7 components, the BLU algorithm does not separate the components corresponding to B–N$^{\pi*}$ and B–N$^{\sigma*}$ although the vacuum signature is still decomposed into two

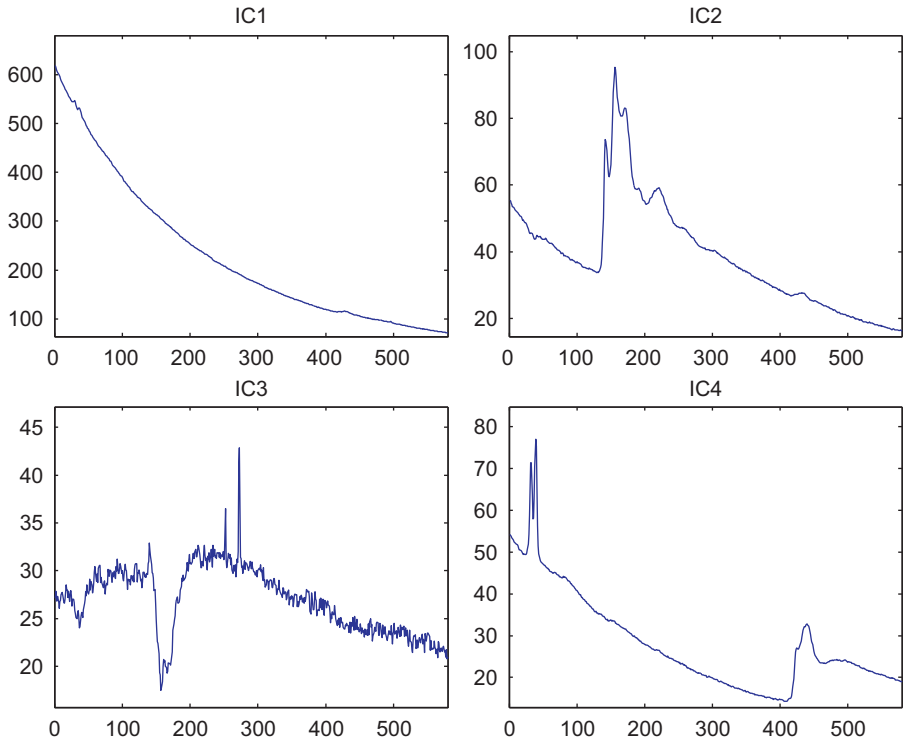

Fig. 8. Spectral components extracted by CubICA with a restricted 430–800 eV energy range. In this case the unmixing is quite satisfactory but only 4 physical EELS spectra are identified. The corresponding maps are depicted in Fig. 9.

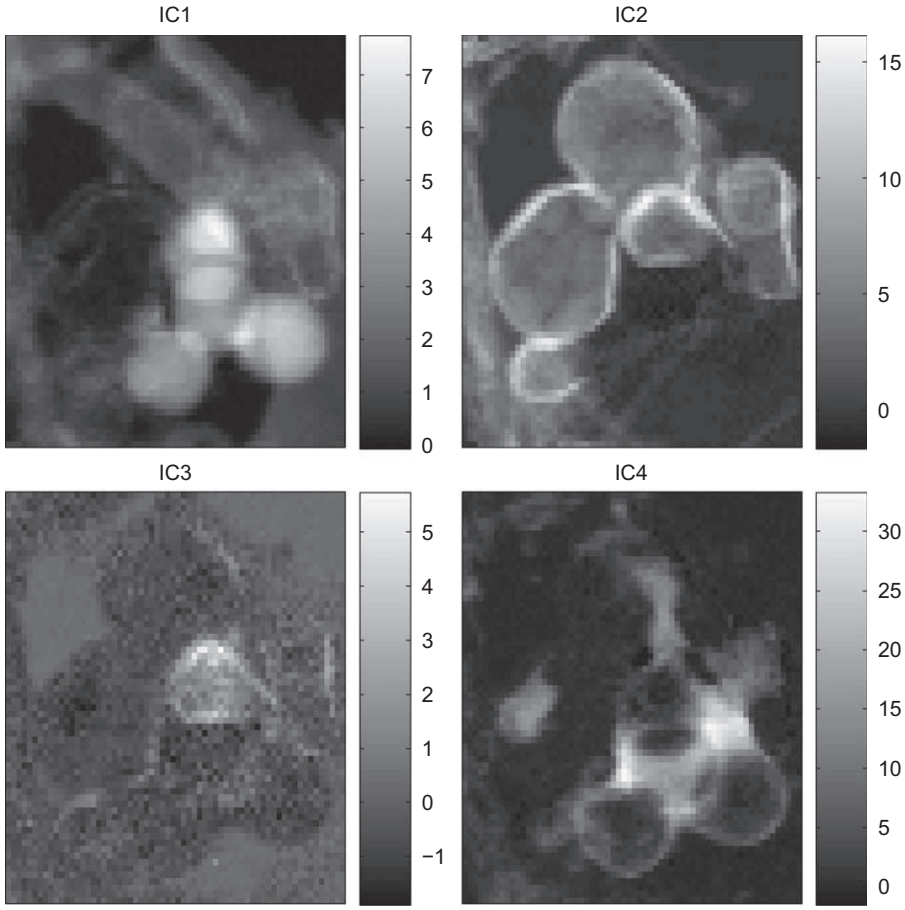

Fig. 9. Maps of the spectral components extracted by CubICA for a limited energy range (the spectral signatures are depicted in Fig. 8).

distinct signatures. Some authors report that some minor components can be masked by the spectral variability of major components [10,15,17]. It can be thus necessary to consider a number of components greater that the number of targets to be identified.

Restricting the analysis to an energy window corresponding to B–K edge does not improve significantly the results. Furthermore, when considering only a restrictive part of the spectra, relevant information composed of the different edges can be lost. For instance, endmember BLU5 with a strong O–K edge is associated with a B–K edge whose fine structure undoubtedly corresponds to B_2O_3. Endmember BLU4 corresponding to a high $\pi*/\sigma*$ ratio for the B–K edge includes a N–K edge with the same feature (Fig. 14).

The maps obtained with BLU seem to be in good agreement with those presented in [14], in particular with a higher intensity of component BLU4 corresponding to particle 2 (particles are located in Fig. 2). The small particle 3 is also better defined with BLU7 than with VCA7. This better agreement of the maps with the one found in [14] illustrate the accuracy of the BLU method when conducting SMA.

4. Discussion

PCA is one of the most commonly used technique to identify significant patterns from multivariate data. As the EELS signatures to be recovered are not orthogonal, components recovered by PCA do not have any physical meaning. As a consequence, it is quite legitimate to conclude that PCA fails to perform interesting spectral unmixing. Nevertheless, since the most relevant components identified by PCA can be used to reconstruct the spectrum-image, PCA can be advocated as a powerful filtering technique, e.g., to denoise the measured signal. Traditional chemical mapping can then be performed on the filtered spectrum-image with a significant increase of the signal-to-noise ratio. However, to go further in the data analysis, it is necessary to resort to more advanced analysis methods.

In [14] bonding maps have been obtained by fitting reference spectra manually extracted from regions of pure compounds. Nevertheless, this supervised method requires a careful inspection of both the elemental maps and the fine structure to correctly select the reference spectra. Advantages of fully unsupervised analysis such as SMA are to rely as little as possible on these subjective choices operated by an expert. In addition, in certain practical circumstances, these choices can be not straightforward. For instance, the pure boron map of [14] actually corresponds to 2 distinct components identified when conducting SMA (BLU2 and BLU6). Consequently, in this typical case, it would be difficult to decide which component should be chosen as a reference for the least square fitting method employed in [14].

In various application fields, ICA has been considered as an efficient tool to extract sources from mixed signals. Plenty of ICA-based methods have been proposed in the literature, and numerous toolboxes are even freely available. These matrix factorization techniques rely on the independence of the signatures to be recovered. However, independence is rather a stringent condition in the targeted application focused in this paper. Indeed, EELS spectrum-images seldom fulfill this critical requirement. Consequently, even if ICA has provided interesting results in some specific cases [7,18], components extracted by this methodology have been demonstrated to be difficulty interpretable.

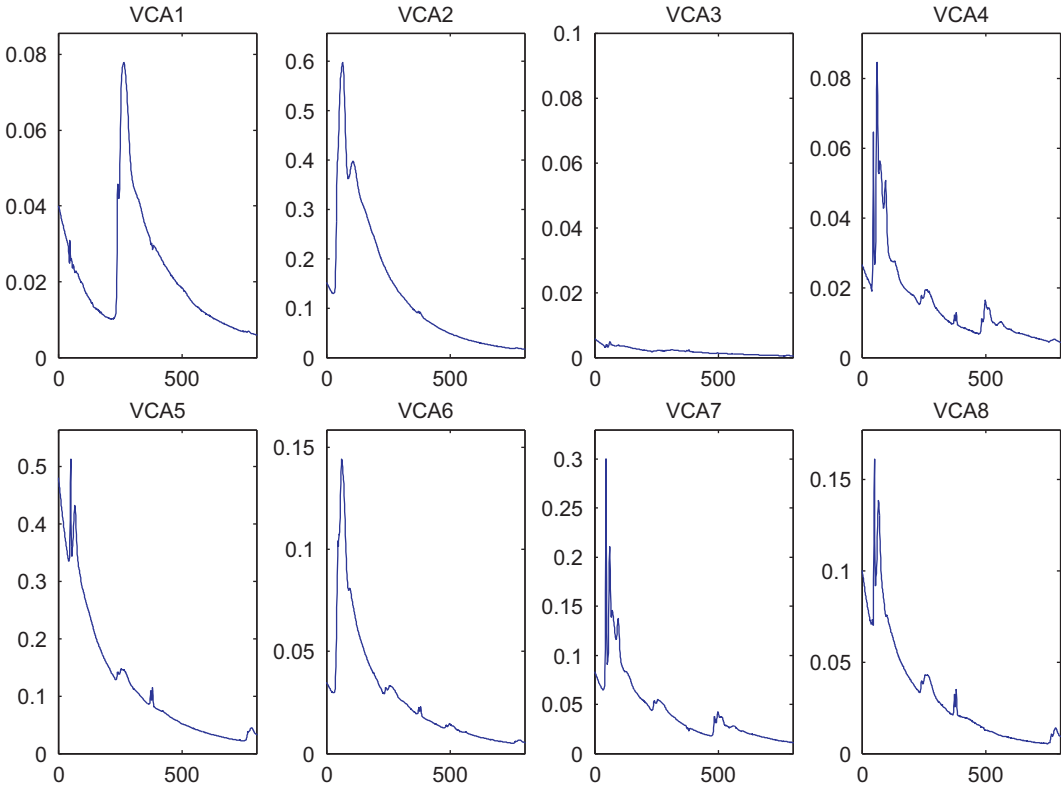

Fig. 10. Spectral components extracted by VCA. These endmembers can be identified as real spectral, since they are chosen among the observed pixels. The corresponding maps are depicted in Fig. 11.

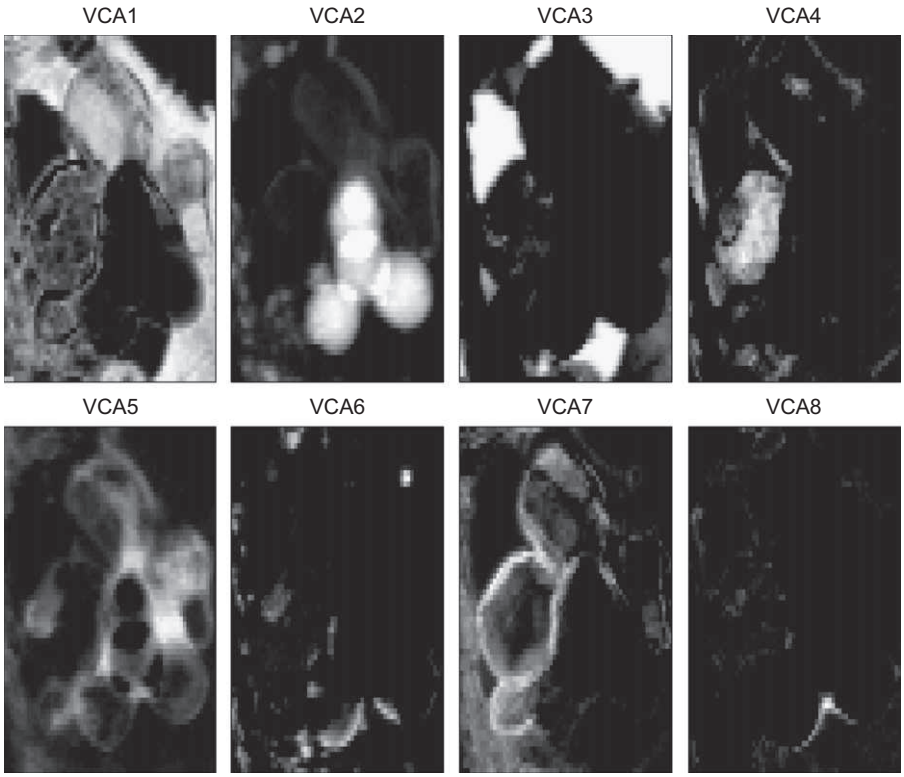

Fig. 11. Maps of the spectral components extracted by VCA (the spectral signatures are depicted in Fig. 10).

Contrary to PCA and ICA, SMA does not require any orthogonality or independence assumptions on the components. Conversely, by explicitly constraining the signatures to be non-negative and the abundances to be related to proportions (i.e., with sum-to-one and positivity constraints), SMA allows the interpretability of the identified patterns to be guaranteed. The statistical BLU algorithm, designed to perform SMA, was able to extract endmembers close to the reference spectra manually extracted in [14]. Contrary to VCA

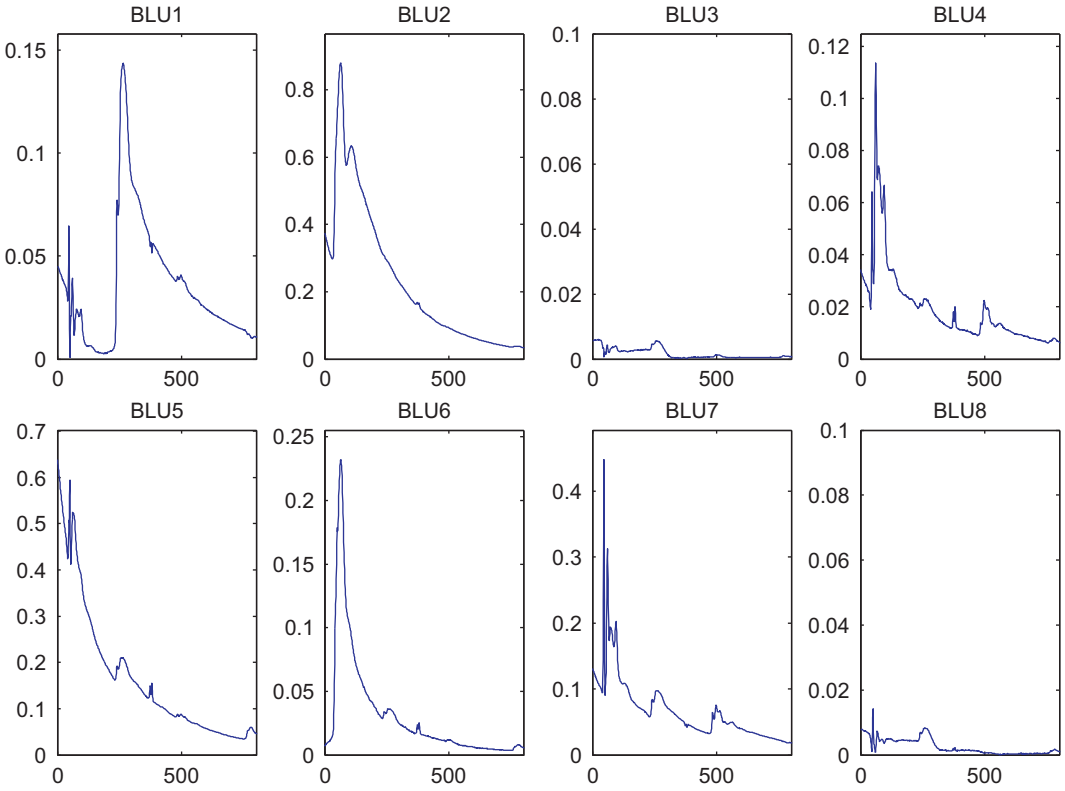

Fig. 12. Spectral components estimated by BLU. The recovered endmembers properly correspond to EELS spectra. Contrary to VCA, these signatures are not initially present in the measures EELS spectrum-image. Indeed, BLU does not require the assumption of the presence of pure pixels in the analyzed image. The corresponding maps are depicted in Fig. 13.

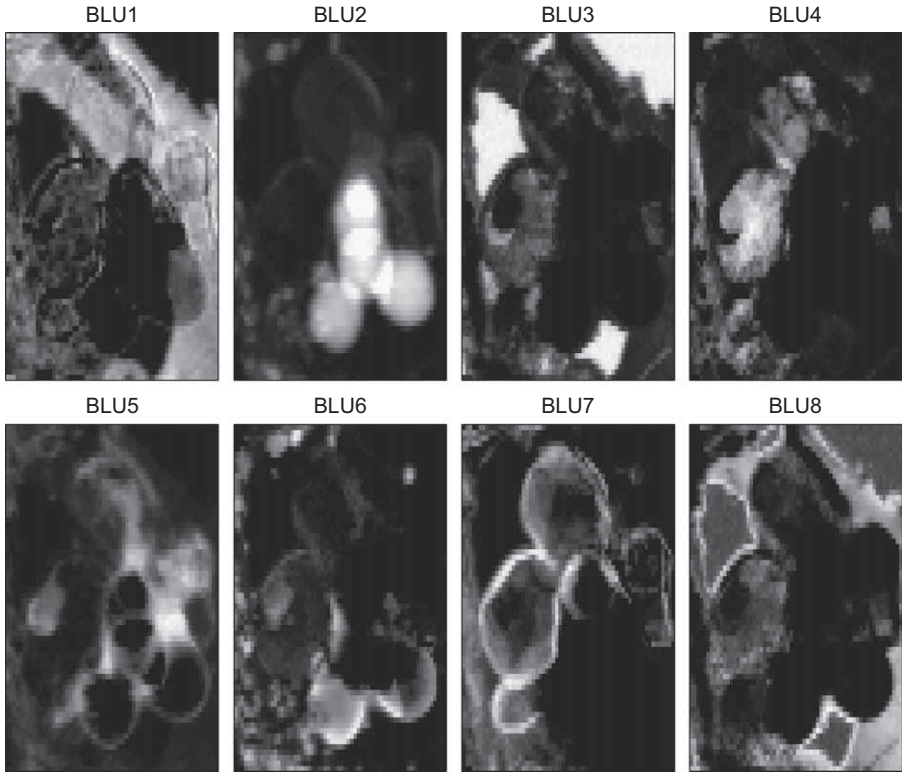

Fig. 13. Maps of the spectral components estimated by BLU (the spectral signatures are depicted in Fig. 12).

which is a geometrical unmixing method, BLU does not require the presence of pure pixels in the analyzed spectrum-image, i.e., pixels composed of a unique endmember. Consequently, BLU has demonstrated undeniable abilities to extract relevant components from EELS spectrum image, and to provide an accurate mapping of these components over the sample.

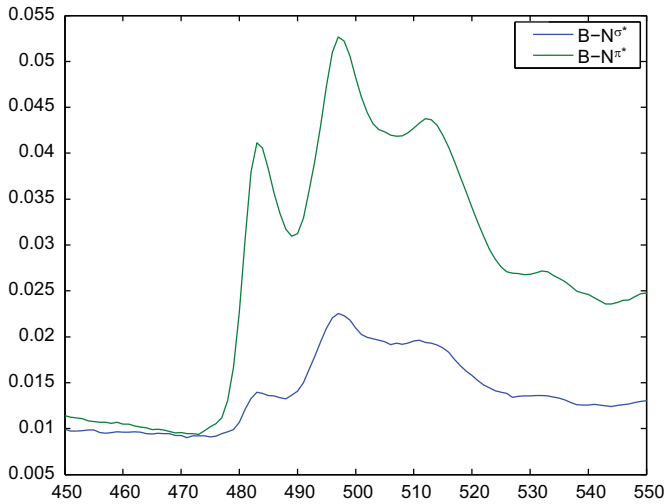

Fig. 14. Detail of the N K edge, with subtracted background and scaled intensities, for endmembers BLU4 (B–N$^{\sigma*}$) and BLU7 (B–N$^{\pi*}$).

5. Conclusions

This work demonstrated the interest of using spectral unmixing, initially devoted to remote sensing images, to perform fine structure analysis of EELS spectrum-images. Several unmixing methods, namely VCA and BLU, were presented as alternative analysis methods to PCA, ICA or least square fitting. According to the conducted study, VCA algorithm was noteworthy for its low computational complexity and could be used on line for a first check of the data during the STEM experiments. At a higher computational price, BLU provided a finer and more relevant mapping of the spectral components. In particular, obtained results were all the more promising as the studied sample was rather complicated, with the presence of vacuum, amorphous carbon support, contamination unexpected elements as Ca.

Spectral mixture analysis, and more specifically the BLU algorithm, represents a significant step in the evolution of the multivariate analysis methods able to extract relevant information from EELS data. More generally, SMA brings an efficient solution to the crucial issue that consists of processing an increasing amount of collected data—in 1998 the data set consisted of only 64 spectra [3], whereas spectrum images of 128×128 pixels are now frequently acquired. One of the main advantages of spectral unmixing methodology is its ability of providing more detailed and more interpretable information about the fine structure of the edges. This work significantly widens the range of analysis methodologies available for the EELS community.

Acknowledgments

The authors would like to thank O. Stephan and R. Arenal for providing the EELS data.

References

[1] C. Colliex, M. Tencé, E. Lefèvre, C. Mory, H. Gu, D. Bouchet, et al., Electron energy loss spectrometry mapping, Microchimica Acta 114 (1994) 71–87.
[2] T.J. Pennycook, M.P. Oxley, J. Garcia-Barriocanal, F.Y. Bruno, C. Leon, J. Santamaria, et al., Seeing oxygen disorder in YSZ/SrTiO colossal ionic conductor heterostructures using EELS, European Physical Journal—Applied Physics 54 (2011) 33507.
[3] N. Bonnet, N. Brun, C. Colliex, Extracting information from sequences of spatially resolved EELS spectra using multivariate statistical analysis, Ultramicroscopy 77 (1999) 97–112.
[4] The HREM Research Inc. website. Available online: 〈http://www.hremresearch.com/〉.
[5] M. Bosman, M. Watanabe, D.T.L. Alexander, V.J. Keast, Mapping chemical and bonding information using multivariate analysis of electron energy-loss spectrum images, Ultramicroscopy 106 (2006) 1024–1032.
[6] N. Bonnet, D. Nuzillard, Independent component analysis: a new possibility for analysing series of electron energy loss spectra, Ultramicroscopy 102 (2005) 327–337.
[7] F. de la Peña, M.-H. Berger, J.-F. Hochepied, F. Dynys, O. Stephan, M. Walls, Mapping titanium and tin oxide phases using EELS: an application of independent component analysis, Ultramicroscopy 111 (2011) 169–176.
[8] B.S. Guiton, V. Iberi, S. Li, D.N. Leonard, C.M. Parish, P.G. Kotula, et al., Correlated optical measurements and plasmon mapping of silver nanorods, Nano Letters 11 (2011) 3482–3488.
[9] M.R. Keenan, Exploiting spatial-domain simplicity in spectral image analysis, Surface and Interface Analysis 41 (2009) 79–87.
[10] N. Keshava, J.F. Mustard, Spectral Unmixing, IEEE Signal Processing Magazine 19 (2002) 44–57.
[11] J.M. Bioucas-Dias, A. Plaza, N. Dobigeon, M. Parente, Q. Du, P. Gader, J. Chanussot, Hyperspectral unmixing overview: geometrical, statistical, and sparse regression-based approaches, IEEE Journal of Selected Topics in Applied Earth Observations and Remote Sensing 5 (2012) 354–379.
[12] N. Dobigeon, S. Moussaoui, M. Coulon, J.-Y. Tourneret, A.O. Hero, Joint Bayesian endmember extraction and linear unmixing for hyperspectral imagery, IEEE Transactions on Signal Processing 57 (2009) 4355–4368.
[13] J. Nascimento, J. Bioucas-Dias, Vertex component analysis: a fast algorithm to unmix hyperspectral data, IEEE Transactions on Geoscience and Remote Sensing 43 (2005) 898–910.
[14] R. Arenal, F. de la Peña, O. Stéphan, M. Walls, M. Tencé, A. Loiseau, et al., Extending the analysis of EELS spectrum-imaging data, from elemental to bond mapping in complex nanostructures, Ultramicroscopy 109 (2008) 32–38.
[15] C.-I Chang, Q. Du, Estimation of number of spectrally distinct signal sources in hyperspectral imagery, IEEE Transactions on Geoscience and Remote Sensing 42 (2004) 608–619.
[16] J. Nascimento, J. Dias, Does independent component analysis play a role in unmixing hyperspectral data? IEEE Transactions on Geoscience and Remote Sensing 43 (2005) 175–187.
[17] C.-I Chang, S.S. Chiang, J.A. Smith, I.W. Ginsberg, Linear spectral random mixture analysis for hyperspectral imagery, IEEE Transactions on Geoscience and Remote Sensing 40 (2002) 375–392.
[18] S. Trasobares, M. López-Haro, M. Kociak, K. March, F. de La Peña, J.A. Perez-Omil, et al., Chemical imaging at atomic resolution as a technique to refine the local structure of nanocrystals, Angewandte Chemie International Edition 50 (2011) 868–872.